Proceedings of the 10th World Congress on Civil, Structural, and Environmental Engineering (CSEE 2025)
Barcelona, Spain - April, 2025
Paper No. ICGRE 140
DOI: 10.11159/icgre25.140

Application of the Kondner model for Predicting Peak Shear Strength in Multistage Direct Shear Tests

María José Toledo Arcic[1], Jens Engel[1]
[1]University of Applied Sciences Dresden HTWD
Friedrich-List-Platz 1, Dresden, Germany
mariajose.toledoarcic@htw-dresden.de; jens.engel@htw-dresden.de

Abstract – This study presents a novel model for predicting the shear strength of fine-grained, coarse-grained, and mixed-grain soils in direct shear tests. The model extrapolates shearing data to predict peak shear strength and displacement before the peak is reached, which is essential for conducting multistage direct shear tests. Although frame shear tests are not element tests, the study demonstrates that the shear stress-strain curve leading up to failure can be accurately approximated using the provided normalized hyperbolic function. The model, developed based on 484 direct shear test results and subsequently validated, utilizes the parameters *a* and *b* of the hyperbolic function, which are determined via a stochastic optimization algorithm to predict peak shear strength effectively.

***Keywords*:** direct shear tests, shear strength prediction, multistage tests, Kondner model, stochastic optimization algorithm, peak shear strength

1. Introduction

Conventional direct shear testing typically requires three single-stage tests to determine a soil's shear strength, ideally using identical soil samples. However, this process can be time-consuming and costly for coarse and, mixed-grained soils due to the need for large-scale equipment and significant material consumption. The multistage direct shear test offers a more efficient alternative for evaluating shear strength [1-6]. However, shear tests must be carefully managed, particularly in dense soils, to guarantee accurate results and avoid damage to the shear zone. To prevent a reduction in shear strength in the shear zone, it is important to apply different termination criteria for the first and second shear phases [1-6].

Preliminary studies and published results [1-6] indicate that stopping the shearing phase in the first and second stages before reaching the peak state is essential for obtaining valid results in multistage tests. Strength components, such as structural integrity, internal bonding, or dilatancy, may only be present during the first shear phase, leading to differences when compared to multistage methods, where these components may no longer be present in subsequent phases [15]. As a result, multistage tests are often avoided. However, investigations have shown that reducing mobilization during a shear stage can minimize its impact on the peak shear strength measured in subsequent stages. The mobilization curve to failure can be predicted before the actual failure occurs. Therefore, the test control must minimize sample perturbations and ensure accurate peak prediction.

This study introduces a model designed to predict peak shear strength in direct shear tests, specifically developed for application in multistage tests. The model was developed from 484 direct shear test results on 175 soils across 6 different soil groups (GW, GP, GM/GC, SP, SM/SC, and CL) and is based on Kondner's (1963) [7] hyperbolic function. The model demonstrated predictive solid accuracy when compared to real test results.

2. Analysis of shear test behaviour

Kondner (1963) [7] introduced a hyperbolic function to approximate the stress-strain curves in conventional drained triaxial tests. Duncan and Chang (1970) [8] later incorporated this approach into an elastoplastic material model, which has since been adapted and extended in various forms (e.g., [11-14]). This approach describes the mobilization of deviator stress (q) as a function of axial strain (ε) using the following Eq. (1):

$$q = \sigma_1 - \sigma_3 = \frac{\varepsilon}{a + b \cdot \varepsilon} \tag{1}$$

where q is the deviator stress, σ_1 and σ_3 are the principal stresses, ε represents the axial strain, and a and b are constants derived from regression analysis of experimental data.

As axial strain increases, the deviator stress reaches an asymptotic limit (q_a) described by:

$$q_a = (\sigma_1 - \sigma_3)_a = \lim_{\varepsilon \to \infty} (\sigma_1 - \sigma_3) = \frac{1}{b} \tag{2}$$

where q_a is the asymptotic deviator stress, σ_1 and σ_3 are the principal stresses, and b is a constant as previously defined.

The asymptotic deviator stress (q_a) is related to the failure deviator stress (q_f) through the failure ratio R_f. A typical value for R_f is 0.9, but for most soils, it falls between 0.75 and 1.0 [10]. The relationship is expressed as:

$$q_a = \frac{q_f}{R_f} = \frac{(\sigma_1 - \sigma_3)_f}{R_f} \tag{3}$$

where q_f and $(\sigma_1 - \sigma_3)_f$ represent the failure deviator stress, and R_f is the failure ratio, which is less than or equal to 1.0.

The constant a in Eq. (1) is the inverse of the initial elastic modulus (E_i) at the beginning of the shearing phase. By substituting Eqs. (2) and (3) into Eq. (1), the following expression is obtained:

$$q = \sigma_1 - \sigma_3 = \frac{\varepsilon}{\frac{1}{E_i} + \frac{\varepsilon}{\frac{(\sigma_1 - \sigma_3)_f}{R_f}}} \tag{4}$$

where q is the deviator stress, σ_1 and σ_3 are the principal stresses, ε represents the axial strain, E_i represents the initial elastic modulus, $(\sigma_1 - \sigma_3)_f$ is the failure deviator stress, and R_f is the failure ratio.

2.1. Application of the model to direct shear tests

Eq. (1) can be applied to direct shear tests by substituting the deviator stress (q) with normalized shear strength (τ_{norm}), and axial strain (ε) with normalized shear displacement ($s_{h,norm}$). In this context, τ_p represents the shear strength at failure, and the subscript p denotes peak values. To fit the model to the experimental data, the shear stresses (τ) and shear displacements (s_h) before reaching the peak are transformed as follows:

$$\tau_{norm} = \frac{\tau}{\tau_p} \qquad \forall \tau \leq \tau_p \tag{5}$$

$$s_{h,norm} = \frac{s_h}{s_{h,p}} \quad \forall s_h \leq s_{h,p} \tag{6}$$

Here, τ_p is the peak shear strength, and $s_{h,p}$ is the shear displacement at τ_p. Eq. (1) can then be expressed as:

$$\tau_{norm} = \frac{s_{h,norm}}{a + b \cdot s_{h,norm}} \tag{7}$$

where τ_{norm} is the normalized shear strength, $s_{h,norm}$ is the normalized shear displacement, and a and b are constants derived from regression analysis of experimental data.

Fig. 1 illustrates an example of normalized data as a solid blue line in the main graph. The inset shows the unnormalized data, with the blue curve representing the data before the peak and the green curve showing the data after the peak.

The evaluation of several individual tests without normalization revealed issues with numerical stability and sensitivity to outliers. Uniform axis scaling facilitates more efficient parameter fitting, which is particularly critical for nonlinear regression models, including the hyperbolic function applied in this study. Section 3 presents the applicability of this model to direct shear tests.

3. Validation of the hyperbolic model in direct shear tests

3.1. Tested materials

A series of tests conducted between 2010 and 2023 in the Geotechnical Laboratory at the University of Applied Sciences Dresden were compiled and systematically evaluated to validate and assess the hyperbolic model applied to direct shear tests. A total of 484 direct shear tests were performed on 175 different soils, using four different devices. All samples were compacted to a relative density between 88% and 100%, with initial moisture content varying from 1% to 54%.

To verify the validity of the hyperbolic model for the direct shear test results, all normalized curves were fitted using Eq. (7).

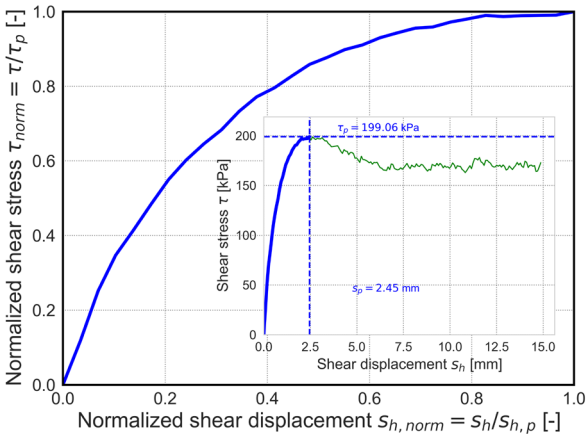

Fig. 1: Normalized shear stress (τ_{norm}) as a function of normalized shear displacement ($s_{h,norm}$) in the direct shear test for sand No. 15830

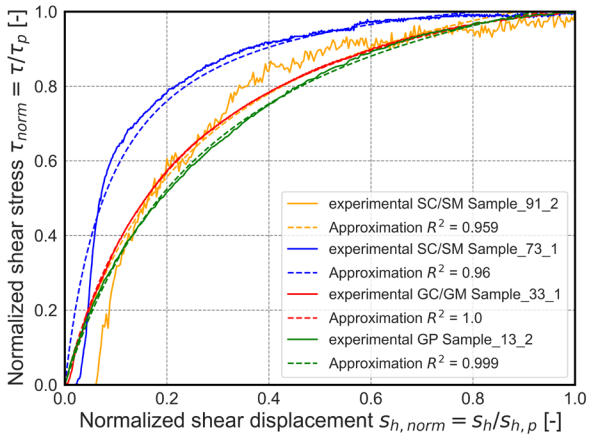

Fig. 2: Selected normalized shear curves (solid lines) and corresponding approximations (dashed lines) according to Eq. (7) from the direct shear tests.

3.2. Test evaluation

The available data enabled the determination of the peak shear strength (τ_p) and the shear displacement at failure ($s_{h,p}$). This allowed for normalization using Eqs. (5) and (6). Equations (2) and (3) are used to calculate the value of R_f based on

the constant b and the parameter τ_p. The constant b represents the asymptote τ_a of the function. R_f plays a crucial role in assessing the validity of the hyperbolic model, as the values obtained from fitting the model should be consistent with those expected based on existing literature.

Fig. 3 presents the distribution of the R_f values obtained. When approximated by a normal distribution, the data mean value of 0.791 and a standard deviation of 0.139, respectively. A comparable study [9] reports R_f values ranging from 0.5 to 1.0 for triaxial tests. The values obtained in this study primarily fall between 0.5 and 1.0, with only 4% of the tests (20 shear tests) yielding values between 0.3 and 0.5. Soils from the GW and GP groups show these lower values. Low R_f values correlate with dense soils, while higher R_f values indicate loosely packed soils.

3.3. Simulation results

In Fig. 2, a selection of normalized shear curves (dashed lines) is presented, alongside their corresponding approximations based on Eq. (7). The orange and blue curves illustrate the two curves with the lowest coefficient of determination (R^2), typically due to fluctuations in the curves. In contrast, the red and green curves represent the two curves with the highest R^2 values.

Fig. 4 provides a histogram of all the R^2 values for the 484 tested samples, including a Weibull distribution with two parameters: scale and shape. The calculated R^2 values range between 0.959 and 1.00, indicating a good fit of the function to the experimental data.

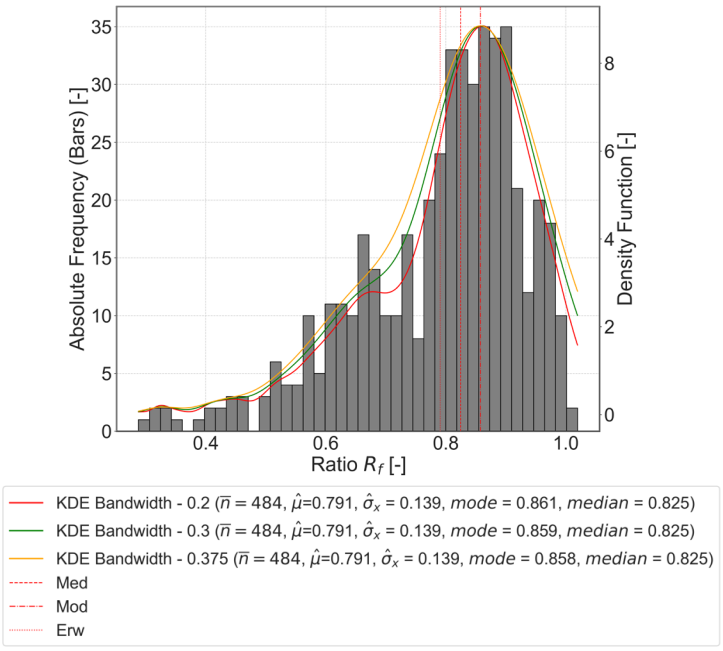

Fig. 3: Representation of the R_f values from the direct shear tests of the 484 samples: Histogram (grey, starting at 0.30, width: 0.018), KDE density function with different bandwidths (red: 0.2, green: 0.3, orange: bandwidth according to Scott, 0.375)

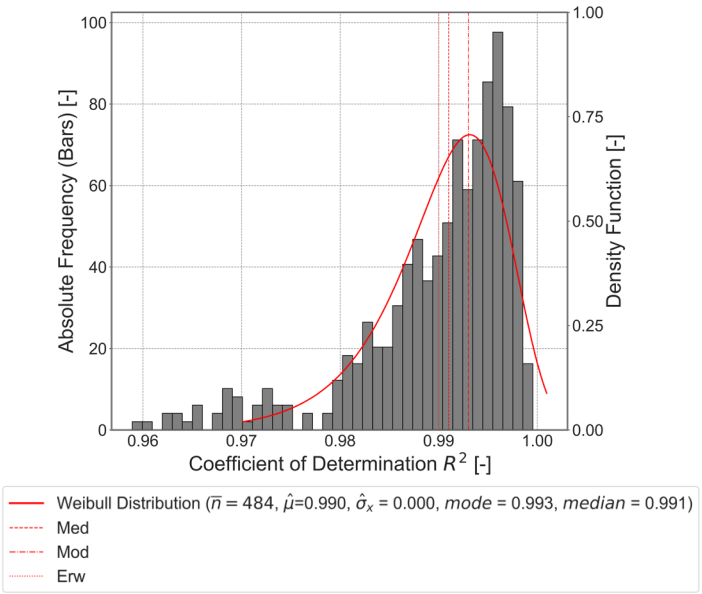

Fig. 4: Representation of the coefficients of determination (R^2 values) for the fitting eq. (8) applied to the 484 shear curves: Histogram (gray, starting at 0.959, width: 0.001), density function: Weibull distribution (scale = 0.993, threshold = 0, shape = 195.71).

Figures 5a and 5b illustrate the constants a and b as functions of the normalized secant elastic modulus $E_{50,norm}$. This modulus refers to the slope between 0 and 50% of the maximum shear stress ($E_{50,norm}$), as expressed in Eq. (8):

$$E_{50,norm} = \frac{\tau_{p,norm}}{2 \cdot s_{h,norm}} = \frac{0.5}{s_{h,norm}} \tag{8}$$

where $E_{50,norm}$ is the normalized secant modulus, $\tau_{p,norm}$ is the normalized peak shear strength, and $s_{h,norm}$ is the the normalized shear displacement.

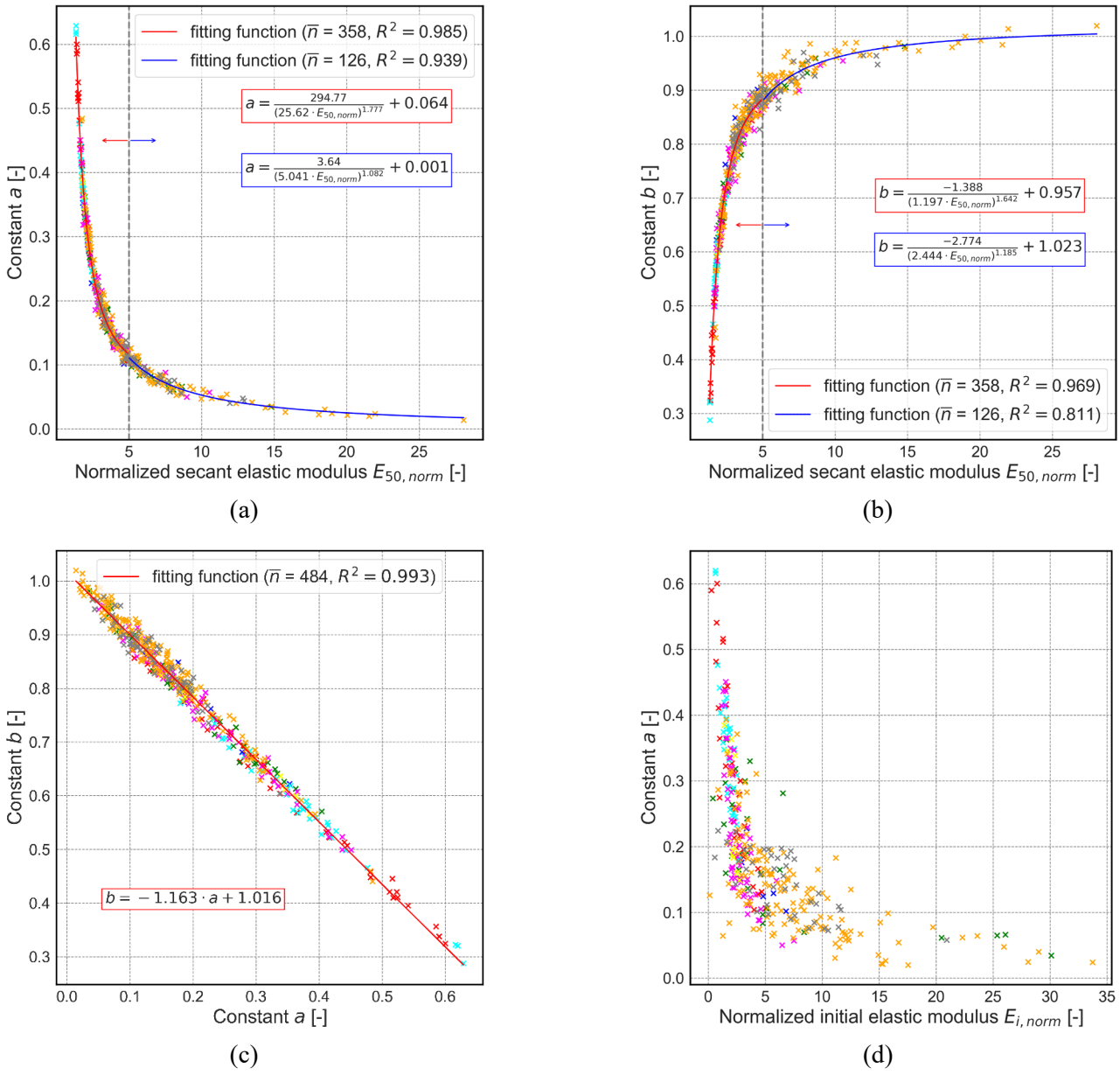

Fig. 5: (a) Dependence of constant a on the normalized secant elastic modulus $E_{50,norm}$ in direct shear tests on 484 investigated samples; (b) Dependence of constant b on the normalized secant elastic modulus $E_{50,norm}$ in direct shear tests on 484 investigated samples; (c) Relationship between constants a and b from the 484 direct shear tests; and (d) Correlation between constant a and the normalized initial stiffness $E_{i,norm}$ in the 484 direct shear tests.

As seen in Fig. 5a, the constant *a* decreases as secant elastic modulus increases. Since a single equation cannot describe all data points, the data were divided into two regions and fitted using regression according to Eq. (9):

$$a\left(E_{50,norm}\right) = \frac{k_1}{\left(k_2 \cdot E_{50,norm}\right)^{k_3}} + k_4 \tag{9}$$

Where $E_{50,norm}$ is the normalized secant modulus and k_1, k_2, k_3, and $k_4$are regression constants.

The first region includes shear curves with normalized secant elastic modulus up to 5 ($E_{50,norm} \leq 5$), while the second region consists of curves with normalized secant elastic modulus greater than 5 ($E_{50,norm} > 5$). In the first region, the constants obtained were k_1 = 294.77, k_2 = 25.62, k_3 = 1.777, and k_4= 0.064, with a coefficient of determination of 0.985. In the second region, the constants were k_1= 3.64, k_2 = 5.041, k_3= 1.082, and k_4= 0.001, yielding a coefficient of determination of 0.939. No correlation was found between compaction ratios or water content before or after compaction.

To perform the regression, the constant *b* was also divided into two regions according to Eq. (9), with the boundary between them set at $E_{50,norm}$= 5. Regression analysis was conducted for each region. The fit (see Fig. 5b) exhibits greater variability in $E_{50,norm}$ for the second range, with a slightly lower coefficient of determination of 0.811. Eq. (10) applies a linear approach to the constants *a* and *b*, with *a* expressed as a function of *b*.

$$a = k_1 \cdot b + k_2 \tag{10}$$

where k_1 and k_2 are regression constants.

Based on Eq. (11) and considering the normalization, where $\tau_{p,norm} = 1$ and $s_{h,norm} = 1$, the relationship between the constants *a* and *b* is expressed as:

$$1 = \frac{1}{\mathrm{a} + \mathrm{b}} \rightarrow \ \mathrm{a} = -\mathrm{b} + 1 \tag{11}$$

The fitting yielded a correlation with a coefficient of determination of 0.993. This linear relationship follows Eq. (10), with the parameters $k_1 = -1.163$ and $k_2 = 1.016$, as shown in Fig. 5c. Fig. 5d compares the constant *b* with the normalized initial elastic modulus ($E_{i,norm}$), showing a weaker correlation, possibly due to the sensitivity of initial elastic modulus calculations influenced by the test equipment. As a result, the attempt to fit these data with a function did not succeed.

Section 4 describes the method for predicting shear strength and summarizes the model's validation results across all direct shear tests.

4. Methodology for predicting peak shear strength

4.1. Basic concept

The primary objective of this study is to develop a reliable method for predicting peak shear strength using an algorithm based on the hyperbolic function introduced earlier, with the parameters *a* and *b* derived in section 3.3. This algorithm processes shear stress and shear displacement data up to a specific level of mobilization, normalizes the data, fits them to the hyperbolic function and then extrapolates the data to estimate the peak values. However, in multistage testing, the first and second shearing phases are terminated before reaching the peak, leaving the maximum shear stress

(τ_p) and the corresponding shear displacement at peak ($s_{h,p}$) unknown. Without these peak values, the normalization of the data is not possible. Therefore, a search algorithm is necessary to estimate τ_p and $s_{h,p}$. The critical parameters for the algorithm are:

- a_F, b_F: Constants determined through regression based on known data, using Eq. (7).
- a_E: Constant derived from $E_{50,norm}$ (determined from known data) using the empirical Eq. (9), with $k_1 = 294{,}77$, $k_2 = 25{,}62$, $k_3 = 1{,}777$, and $k_4 = 0{,}064$ for $E_{50,norm} \leq 5$ and with $k_1 = 3{,}64$, $k_2 = 5{,}041$, $k_3 = 1{,}082$ and $k_4 = 0{,}001$ for $E_{50,norm} > 5$
- b_E: Constant determined from the relationship between the constants *a* and *b*, using the empirical Eq. (10), with $k_1 = -1{,}163$ and $k_2 = 1{,}016$.

This algorithm estimates the unknown values of τ_p and $s_{h,p}$ from the curve section in the normalized shear stress-displacement diagram (a_F, b_F) and compares them with the values derived from $E_{50,norm}$ using empirical equations for *a* and *b*. The evaluation uses the mean squared error (MSE) for different values of τ_p und $s_{h,p}$, as described in Eq. (12). The algorithm uses a stochastic differential evolution process to find the point where the error reaches its minimum.

$$MSE_{mean} = \frac{(a\_F - a\_E)^2 + (b\_F - b\_E)^2}{2} \tag{12}$$

where MSE_{mean} is the mean squared error, a_F and b_F are the constants determined through regression using Eq. (7), and a_E and b_E are derived from the empirical Eqs. (9) and (10).

The algorithm operates with a main function that calls a helper function to perform key tasks, including processing the current shear data, normalizing the data, extracting constants *a* and *b* from the diagrams, curve fitting, and evaluating the fit quality using mean squared error. To ensure effective iterations, it is essential to set reasonable boundaries for τ_p and $s_{h,p}$. For example, the shear displacement data from the third stage of a multistage test can be used as input to estimate the boundaries for phases 1 and 2.

4.2. Validation

Direct shear tests in single-stage provided the basis for the initial validation. This study considers variations in the measured shear stress of approximately ±10% of the peak shear strength (τ_p) as acceptable. The Algorithm evaluated all single-stage tests by comparing the predicted peak shear stresses ($\tau_{p,pred}$) and shear displacements ($s_{h,pred}$) with the measured values. The relative error (RE) is calculated using the following equation:

$$RE[\%] = \frac{(\tau_{p,pred} - \tau_p) \cdot 100}{\tau_p} \tag{13}$$

where RE is the relative error in percentage, $\tau_{p,pred}$ is the predicted peak shear strength, and τ_p is the measured peak shear strength.

The simulations considered shear stresses corresponding to shear displacements of 50%, 55%, 60%, 65%, 70%, 75%, 80%, 85%, and 90% of the peak shear displacement. Fig. 6 presents the simulation results as a normal distribution.

An increase in the dataset narrows the normal distribution curve, reduces the relative error, and improves the accuracy of the simulation results. The narrowing of the distribution around the mean indicates reduced variability in the data points,

which cluster more closely to the expected value. Fig. 7 presents the percentage of tests (100% = 484 tests) that show a relative error greater than 5%, 8%, 10%, and 15% between the predicted and actual peak shear strength. With a stopping point at 60% of the peak shear displacement, fewer than 10% of the tests show a relative error of over 10% between the predicted and actual peak shear strength. This study confirms that the hyperbolic model accurately describes shear in direct shear tests and effectively predicts peak shear strength.

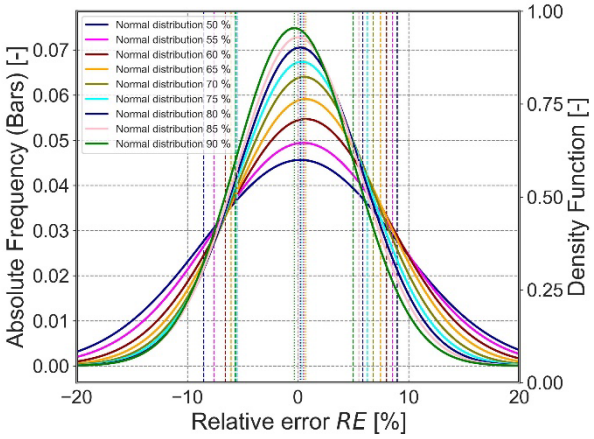

Fig. 6: Representation of the relative error in shear stress calculated according to Eq. (15) for the 484 direct shear tests. Density functions: Normal distribution.

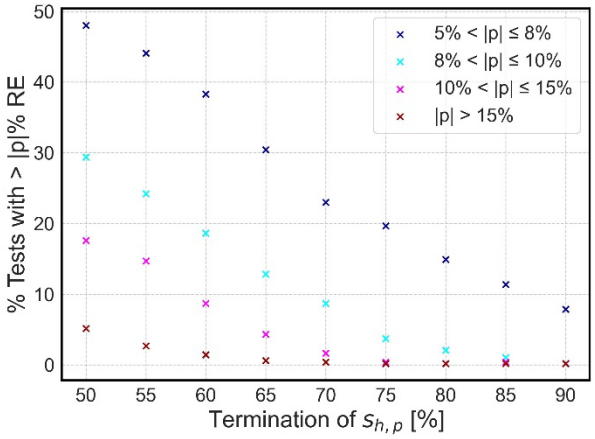

Fig. 7: Summary of the percentages of the 484 tests that exhibit a relative error (RE) exceeding $|p|$%, based on the percentage of the shear displacement at peak ($s_{h,p}$).

5. Conclusion and outlook

This study introduces a new model for predicting the shear stress and shear displacement at the peak state in direct shear tests. The model uses the initial data from the stress-displacement curve and incorporates empirical methods to predict them. It normalized the shear stress-displacement curve up to the peak and fitted the data to a Kondner function. Developed initially for drained triaxial tests, this approach forms the foundation for several material models, including the Hardening Soil or Duncan-Chang models. The two constants, a and b are fundamental to the model, with a strongly correlating with the normalized secant elastic modulus at 50% of the peak shear stress, while b demonstrates a linear relationship with a. By applying these two constants and a newly developed stochastic algorithm based on differential evolution, the model accurately predicts the peak shear strength and the shear displacement at peak.

The model was validated using 484 direct shear tests on different materials to determine the constants a and b, and the results were evaluated against known peak states. After analyzing data from different soil types, the parameters proved applicable across different soil groups. The goal is to establish the optimal stopping point during the shear test as a basis for multistage tests. To achieve this, mobilization curves with displacements between 50% and 90% of the peak shear displacement were compared with the predictions from the new model. The evaluation relied on the stochastic analysis of normal distributions and their deviations, ensuring accuracy within defined limits.

Future research will focus on developing methods to determine the shear strength of soils using multistage tests, aiming to achieve results equivalent to those from single-stage tests. Defining the optimal stopping criterion during the shearing phase is crucial for this goal. The results presented here are based on tests conducted with compacted samples. Additional adjustments will be needed to account for other influencing factors, such as aging or structure.

Acknowledgements

The Federal Ministry for Economy Affairs and Climate Action BMBF (Project number 49VF230003) and Bank of Saxony SAB (Project number 100604731) supported this research financially.

References

[1] S. Nam, M. Gutierrez, P. Diplas and J. Petrie, "Determination of the shear strength of unsaturated soils using the multistage direct shear test," in *Engineering Geology*, 2011, vol. 122, pp. 272-280.

[2] D. Hormdee, N. Kaikeerati and P. Angsuwotai, "Evaluation on the results of multistage shear test," in *International Journal of GEOMATE*, 2012, vol. 2, pp. 140-143.

[3] H. S. Saeedy and M. A. Mollah, "*Application of Multi-Stage Triaxial Test to Kuwaiti Soils,"* in: Donaghe, R.T., Chaney, R.C. and Silver, M.L., Eds., Advanced Triaxial Testing of Soil and Rock, ASTM, Philadelphia.1988, pp. 363-375.

[4] D. Kotsanis, P. P. Nomikos, D. Rozos and A. I. Sofianos, "*Multistage triaxial testing of various rock types: A case study of East Attica Prefecture, Greece,"* in Procedia Structural Integrity, 2018, vol. 10. pp. 112-119.

[5] A. Vakilinezhad1 and N. K. Toker, "*Application and comparison of multistage triaxial compression test procedures on reconstituted Ankara clay*," in *Proceedings of the 3S Web of Conferences 544 IS-Porto 2023*, 2024, vol. 544.

[6] M. J. Toledo Arcic, "Entwicklung einer datenbasierten Steuerung für Scherversuche in Mehrstufentechnik," in Tagungsband der *38. Baugrundtagung, Forum für junge Geotechnik-Ingenieure und -Ingenieurinnen*, Bremen, Germany, 2024, pp. 39-46.

[7] R. L. Kondner, „*Hyperbolic stress-strain response: cohesive soils,"* in: J. Soil Mech. Found., ASCE 89 (SM1), 1963, pp. 115–143.

[8] J. M. Duncan and C. Y. Chang, "*Nonlinear analysis of stress and strain in soil,"* in: Journal of the Soil Mechanics and Foundations Division. ASCE. 1970, Vol. 96. Nr. 5. pp. 1629-1653.

[9] R. Obrzud and A. Truty, "*The Hardening Soil Model– A Practical Guidebook,"* Zace Services Ltd, Software Engineering, Switzerland, 2018, 205 p.

[10] T. Schanz, P. A. Vermeer and B. G. Bonnier, „*The Hardening Soil Model: formulation and verification,"* in: Beyond 2000 in Computational Geotechnics - 10 years of PLAXIS, Balkema, 2000.

[11] T. M. Tharp and M. G. Scarbrough, "*Application of hyperbolic stress–strain models for sandstone and shale to fold wavelength in Mexican Ridges Foldbelt,"* in J. Struct. Geol. 1994, 16(12), pp. 1603–1618.

[12] J. M. Duncan, "*Hyperbolic stress-strain relationships,"* in: Limit Equilibrium, Plasticity and Generalized Stress-Strain in Geotechnical Engineering (edited by Yong, R. K. & Ko, H.-Y.). Am. Soc. Civ. Engr., New York. 1981, pp. 443--460.

[13] J. Habimana, V. Labiouse and F. Decoeudres, "*Geomechanical characterisation of cataclastic rocks: Experience from the Cleuson-Dixence project*," in: Int. J. Rock Mech. Min. Sci. 2012, 39(6), pp. 677–693.

[14] Y. P. Vaid, "*Effect of consolidation history and stress path on hyperbolic stress-strain relations,"* in: Canadian Geotechnical Journal, 1985, 22. pp. 172-176.

[15] M. J. Toledo Arcic, A. Mehrpajouh, C. Lauer, M. Pamler und J. Engel, "*Komplexe Bewertung bodenmechanischer Versuche zur Ermittlung von Kennwerten*," Konstruktiver Ingenieurbau, Bd. 06, pp. 5-10, 2022.